

## Spin-polarized energy-band structure, conduction-electron polarization, spin densities, and the neutron magnetic form factor of ferromagnetic gadolinium\*

B. N. Harmon<sup>†</sup>

*Physics Department, Northwestern University, Evanston, Illinois 60201*

A. J. Freeman

*Physics Department, Northwestern University, Evanston, Illinois 60201  
and Argonne National Laboratory, Argonne, Illinois 60439*

(Received 15 April 1974)

Conduction-electron polarization, spin densities, and neutron magnetic scattering in ferromagnetic Gd metal were studied using the spin-polarized augmented-plane-wave (APW) method in a warped-muffin-tin-potential formulation. The spin-up and spin-down bands were found to be very similar in shape to the bands from a paramagnetic calculation, with the exchange splitting proportional to the amount of  $d$  character in the bands. It was also found that the conduction-electron spin density determined from the APW wave functions is of mostly  $d$  character. This dominance of the  $d$ -like wave functions for the spin-dependent interactions is explained by (i) the much greater overlap of the  $4f$  states with the  $d$ -like wave functions as compared to the  $s$ - $p$  wave functions; (ii) the nearly complete  $d$  character of the bands in the region of the Fermi surface. The magnetic form factor was calculated from the conduction-electron spin density and compared with the recent neutron magnetic-form-factor measurement of Moon, Koehler, Cable, and Child. The calculated spin density was found to have the same shape as the "diffuse" density derived by Moon *et al.* (including a negative but much smaller in magnitude spin density at the  $c$  site in the unit cell). After the inclusion of core-polarization effects we conclude that large nonspherical contributions with  $Y_{33}-Y_{3-3}$ , and  $Y_{40}$  angular dependence are needed to explain the experimental results.

### I. INTRODUCTION

The rare-earth metals are distinguished by their unique and rather unusual magnetic, electric, and optical properties.<sup>1</sup> Extensive studies during the last decade have provided a fairly deep understanding of their electronic structure and properties.<sup>1</sup> The open shell of atomiclike (highly localized)  $4f$  electrons are responsible for their large magnetic moments and their exotic magnetically ordered structures. However, since there is negligible overlap of the  $4f$  shells on neighboring lattice sites, the ordering of the  $4f$  moments is believed to be accomplished through their exchange interaction with the conduction electrons. The coupling between the conduction electrons and the local  $4f$  states is responsible for resistivity anomalies near the magnetic ordering temperatures, and also gives rise to the magnetic polarization of the conduction electrons which affects a variety of other properties.<sup>2</sup>

The conduction-electron band structure of the rare-earth metals has been determined in a number of band-structure studies.<sup>2</sup> The first-band calculations<sup>3,7</sup> showed that the band structures for these metals were similar to those of the transition metals, with high  $d$ -band density of states and with Fermi surfaces unlike those expected for nearly free electrons.<sup>2</sup> There is now sufficient evidence to indicate that the augmented-plane-wave (APW)

method, using a muffin-tin potential and the Slater-exchange approximation, yields a very reasonable energy band structure for the rare-earth metals. The anisotropies in the shape of the calculated paramagnetic Fermi surface have been confirmed by positron annihilation and by resistivity measurements<sup>1,2</sup>; also, the nesting features of the Fermi surface, as calculated using the relativistic-APW method, have been found to correlate well with the observed magnetic ordering.<sup>2</sup> Until recently the difficulty in preparing very pure samples of these metals has prevented detailed comparison of the theory with precise measurements, as, for example, could be obtained from de Haas-van Alphen experiments. Thus the neutron magnetic-form-factor measurement of Gd by Moon, Koehler, Cable, and Child<sup>4</sup> is of great significance, since it is the first precise experiment to give direct information about the conduction-electron magnetization densities in the rare-earths. Gadolinium orders ferromagnetically below 293°K, with a total magnetic moment of  $7.55\mu_B$ /atom in high fields. The  $0.55\mu_B$ /atom above the  $7\mu_B$ /atom expected from the seven unpaired  $4f$  electrons is due to the polarization of the conduction electrons. In the analysis of their experimental results, Moon *et al.*<sup>4</sup> separated from the total form factor a spherical contribution representing the localized  $4f$  electrons and obtained a form factor which is presumably due to the diffuse distribution of the polarized con-

duction electrons. A principle motivation for our work is to understand from *ab initio* calculations this diffuse form factor, the conduction-electron spin density, and the  $4f$ -conduction-electron interactions responsible for it. The lack of previous investigations into the ferromagnetic nature of the conduction-electron wave functions in the rare-earth metals necessitated an exploratory approach to these interesting questions. For this reason, detailed agreement with experiment was not a goal of these calculations, nor was it expected.

The spin-polarized APW method was chosen for computation of the spin density for several reasons: (i) The ferromagnetic band structures of the transition metals have been successfully obtained using this method; (ii) the APW paramagnetic Fermi surfaces have been shown by experiments to be reasonable; (iii) the nonrelativistic paramagnetic band structure of Gd is in essential agreement with the relativistic result; (iv) spin is maintained as a good quantum number in the nonrelativistic regime. We computed the bands, wave functions, and densities using two different values of the Slater exchange parameter  $\alpha$ . Since the best agreement with experiment was obtained with the  $\alpha = 1$  calculation, we describe the results obtained using that value of exchange and only briefly mention the results from the  $\alpha = \frac{2}{3}$  calculation. For details of all these calculations the reader is referred to Ref. 5.

In Sec. II we describe the character of the spin-polarized bands and wave functions, and in Sec. III we discuss and compare the theoretical and experimental spin densities and form factors. Additional contributions to the magnetization density and the magnetic form factor are considered in Sec. IV and conclusions are then given in Sec. V.

## II. ENERGY-BAND AND WAVE-FUNCTION PROPERTIES OF FERROMAGNETIC Gd METAL

The electronic band structures of the rare-earth metals in general and Gd metal in particular have been determined<sup>2</sup> first by means of nonrelativistic<sup>3,6</sup> and later by relativistic energy-band calculations.<sup>7</sup> These extensive studies showed that the conduction bands in these hcp metals are identical with those of the  $3d$  transition metals having the hcp structure, namely, overlapping  $s$ -like and  $d$ -like bands which are strongly hybridized. In all these investigations, the APW method<sup>8</sup> was employed to determine the band structure, density of states, and Fermi surface of the paramagnetic metals. The spin-polarized version of the APW method has also been successfully used to calculate the band structures of the ferromagnetic transition metals.<sup>9</sup> Since excellent reviews of the APW meth-

od have been given,<sup>10-12</sup> only those aspects of the method important for obtaining and utilizing wave functions will be presented in this paper.

The APW method has considerable intuitive appeal. As is well known, the one-electron states of the crystal are expanded in atomiclike functions for regions near the atomic sites, and in plane waves for regions in the unit cell away from the atomic sites. This basis is physically reasonable and results from considering the crystal potential in the muffin-tin approximation. In this approximation the unit cell is separated into two regions by nonoverlapping spheres surrounding each atomic site. Inside each sphere the potential is assumed spherically symmetric, and appears quite atomiclike; outside the spheres the potential is assumed constant. It is easy to avoid this last assumption and include the general potential outside the spheres. This so-called warped-muffin-tin (WMT) potential<sup>13</sup> is easy to incorporate into the APW formalism and has been used in our calculations (see the Appendix).

A crystal wave function is expanded in augmented plane waves as

$$\psi_{\vec{k}, E}(\vec{r}) = \sum_{\vec{k}_i} A_i(\vec{k}) \varphi_{\vec{k}_i}(\vec{r}), \quad (1)$$

with the coefficients  $A_i(\vec{k})$  to be determined variationally. The sum is over a set of reciprocal-lattice vectors  $\vec{K}_i$ , where we have written  $\vec{k}_i$  for  $\vec{k} + \vec{K}_i$ . An APW has the following representation:

outside the spheres,

$$\varphi_{\vec{k}_i}(\vec{r}) = (1/\sqrt{\Omega}) e^{i\vec{k}_i \cdot \vec{r}}, \quad (2)$$

where  $\Omega$  is the volume of the unit cell;

inside the  $\nu$ th sphere,

$$\varphi_{\vec{k}_i}(\vec{r}) = e^{i\vec{k}_i \cdot \vec{r}_\nu} \sum_{l, m} A_{lm}(\vec{k}) R_{l, E}(\rho) Y_{lm}(\hat{\rho}), \quad (3)$$

$$|\hat{\rho}| = |\vec{r} - \vec{r}_\nu| < R_\nu,$$

where  $R_\nu$  is the radius of the sphere, and  $\vec{r}_\nu$  is the vector to the center of the sphere.

The  $A_{lm}$  are chosen so that each APW basis function is continuous at the sphere boundary. This guarantees that the crystal wave function will be continuous; there will remain, however, a slope discontinuity since we are limited to a finite expansion. The  $R_{l, E}(\rho)$  are the radial solutions to Schrodinger's equation inside the APW sphere.

$$\left[ -\frac{1}{r^2} \frac{d}{dr} \left( r^2 \frac{d}{dr} \right) + \frac{l(l+1)}{r^2} + V(r) - E' \right] R_{l, E}(\rho) = 0. \quad (4)$$

The  $R_{l, E}(\rho)$  must be regular at the origin, but unlike the atomic case there is no boundary condi-

tion at infinity and hence there exist solutions for all values of  $E$ . The proper creation of the potential in this equation is of the utmost importance if physically meaningful results are to be obtained. The wave function and eigenvalue are determined by the Rayleigh-Ritz variational procedure as solutions of a standard eigenvalue problem. As discussed in Refs. 10 and 11, the APW secular equation can be solved by finding those  $E_i$  which satisfy

$$\det |\underline{H}(E_i) - E_i \underline{S}| = 0. \quad (5)$$

This procedure is useful for finding the eigenvalues, but is not as convenient for obtaining wave functions. One problem with obtaining eigenvectors is that the normalization is over the region outside the spheres and not over the unit cell. Since we are primarily concerned with obtaining normalized wave functions, it is best to employ the linearized form of the APW method as given by Koelling<sup>14</sup> to solve the equation

$$\underline{H}(E_0) \underline{\tilde{A}} = E \underline{S}(E_0) \underline{\tilde{A}}, \quad \underline{S} = \text{total overlap matrix.} \quad (6)$$

The procedure is to pick an  $E_0$  and evaluate the resulting eigenvalues  $E_i$ , by the method discussed below. If one of the  $E_i$  is equal to  $E_0$  then the wave function is evaluated. If  $E_0$  does not equal any  $E_i$ , then  $E_0$  is set equal to one of the  $E_i$  found, and an iteration performed. In practice this procedure converges very rapidly.<sup>15</sup>

Equation (6) is solved by using Cholesky factorization of the overlap matrix,<sup>15</sup>

$$\underline{S} = \underline{L} \underline{L}^T. \quad (7)$$

The new eigenvalue equation is then

$$(\underline{L}^{-1} \underline{H} \underline{L}^{-T}) (\underline{L}^T \underline{\tilde{A}}) = E (\underline{L}^T \underline{\tilde{A}}) \quad (8)$$

or

$$\underline{H}' \underline{\tilde{A}}' = E \underline{\tilde{A}}'. \quad (9)$$

The new matrix  $\underline{H}'$  is reduced to tridiagonal form using the Housholder-Givens method,<sup>16</sup> and a Sturm sequencing procedure is used to evaluate the needed eigenvalues. Usually only the 6–10 lowest eigenvalues are obtained. If the whole spectrum (actually 25% of the eigenvalues or more) is needed it is more efficient to employ a  $QL$  algorithm instead of the Sturm sequence procedure. Once the eigenvalues are determined, the eigenvectors are easily obtained by back transformations. These procedures are fully discussed by Wilkinson,<sup>16</sup> and are available through the EISPAC set of subroutines.

The crystal potentials for the spin-up and spin-down bands were obtained by using Mattheiss's prescription of superimposing atomic charge densities from neighboring sites.<sup>17</sup> The atomic den-

sities were determined from a self-consistent spin-polarized Hartree-Fock-Slater calculation with the assumed atomic configuration  $4f^7, 5d_1^{0.5}, 5d_2^{0.5}, 6s^2$ . (When the atomic configuration  $5d_1^{0.775}, 5d_2^{0.225}, 6s^2$  was picked to represent the metal with a net magnetic moment of  $0.55 \mu_B/\text{atom}$ , it was found that with the full Slater exchange this configuration gave much too large a band splitting.) Since the wave functions were found to be sensitive to non-muffin-tin corrections, we used the so-called warped-muffin-tin potential (see the Appendix). For each of the potentials considered, the spin-polarized energies and wave functions were calculated on a  $\pi/4a, \pi/2c$  mesh in the irreducible  $\frac{1}{24}$  of the Brillouin zone.

The calculated spin-up and spin-down bands were found to be nearly identical to the nonrelativistic paramagnetic band structure of Dimmock, Freeman, and Watson,<sup>6</sup> and, as these authors found, the bands were rather insensitive to changes in potential. The relative positions of the two sets of bands caused by the ferromagnetic exchange splitting is shown along the  $T$  symmetry line in Fig. 1. An important feature to note is the smaller splitting of the  $s$ -like band near  $\Gamma$ , as compared to the splitting of the bands with strong  $d$  character. Also present, but less obvious, is the increase of the splitting for the  $d$  bands as the energy eigenvalue increases. (The spin-up and spin-down bands obtained from the  $\alpha = \frac{2}{3}$  potential were also found to be very similar in shape. The relativistic paramagnetic band structure,<sup>7</sup> except for fewer band crossings caused by symmetry, like-

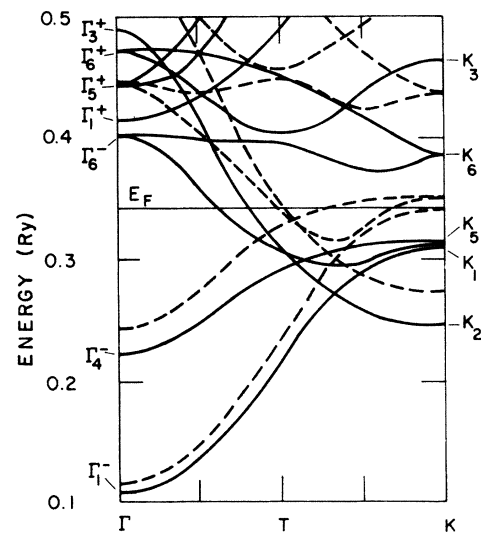


FIG. 1. Spin-up (solid curves) and spin-down (dashed curves) energy bands in ferromagnetic Gd metal plotted along  $\Gamma$  to  $K$ .

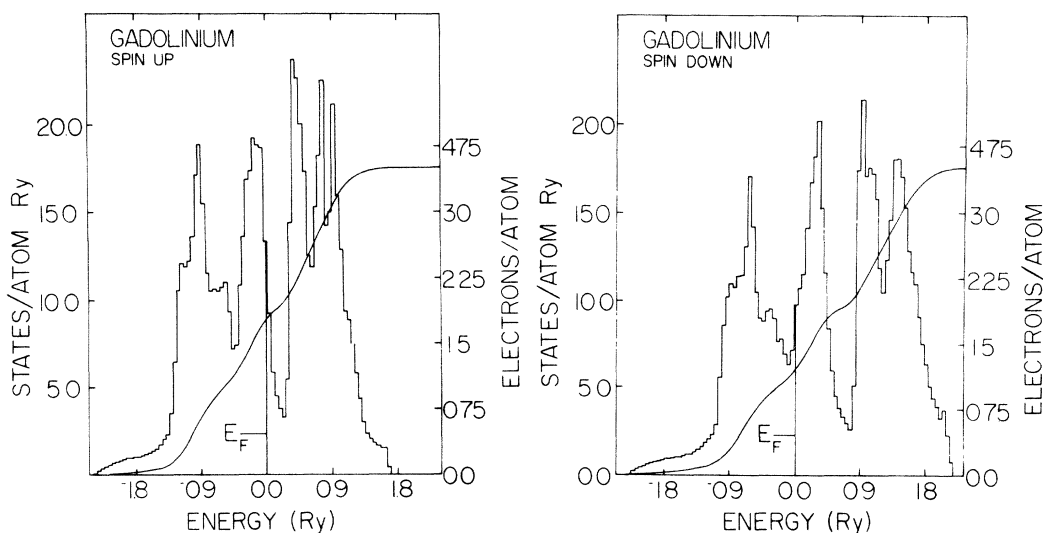


FIG. 2. Spin-up and spin-down density of states for ferromagnetic gadolinium.

wise resembles the nonrelativistic structure. Again one may conclude, as did Dimmock *et al.*,<sup>6</sup> that the general features of the band structure are insensitive to potential changes.)

The density of states for the  $\alpha = 1$  potential is shown in Fig. 2. Here too, there is great similarity between the spin-up and spin-down density of states, and the paramagnetic relativistic and nonrelativistic density of states (the *s* band density is slightly lower in energy for the relativistic density of states).<sup>7</sup> The Fermi level shown in Fig. 2 was determined by filling the bands with six electrons per unit cell. There were 3.72 spin-up electrons and 2.28 spin-down electrons yielding a net magnetic moment of  $0.72\mu_B/\text{atom}$ . This is  $0.17\mu_B$  above the experimental value and indicates too large an exchange splitting near the Fermi energy. It is also possible that calculating the energies on a higher density mesh would yield a slightly different density of states and Fermi level. This could change the net magnetic moment, but it is doubtful that the moment would change by more than  $0.05\mu_B$ . Since the band shape was relatively insensitive to the potential changes, a new calculation with an improved potential was not performed. Rather, the spin-up bands were rigidly shifted by 0.012 Ry and the spin-down bands by 0.006 Ry to obtain the experimental moment of  $0.55\mu_B/\text{atom}$ . An average splitting before shifting was about 0.8 eV, and after shifting 0.57 eV. Optical experiments indicate the splitting to be about 0.7 eV. At this experimental splitting the calculated magnetic moment would be too large; however, this could be because the calculation is nonrelativistic. The true relativistic bands may have some spin admixture

and thus require larger splittings to obtain the same moment. It is also possible that the orbital moment of the conduction electrons points in the direction opposite to the direction of the spin moment. Then if the conduction-electron orbital moment due to spin-orbit coupling were large, the bands would be split more than would be predicted by the measured saturated moment. Small shifts in the band splitting will affect the magnitude of the spin magnetic moment, but should not change the magnetic form factor appreciably.

Consider now the resulting eigenfunctions and spin densities. For comparison with the band results and because it gives some insight into the behavior expected (and found) for the wave functions in the solid we show in Fig. 3 the spin-polarized 5*d* radial functions obtained from an atomic calculation for Gd. (Also shown in the figure is

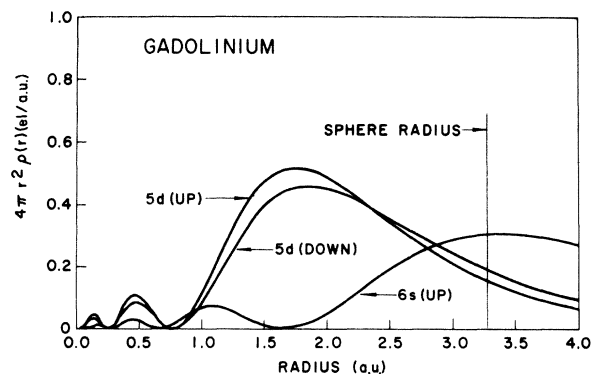


FIG. 3. Spin-polarized 5*d* orbitals and the spin-up 6*s* orbital of atomic gadolinium.

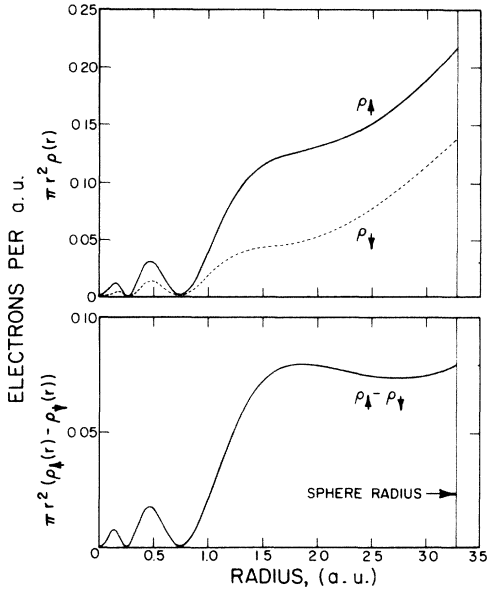


FIG. 4. APW spherical charge and spin densities of ferromagnetic gadolinium.

the spin-up  $6s$  orbital and the position of the sphere radius.) The peak in the well-localized  $4f$  density is located near  $r=0.7$  Bohr radii, well inside the outer maximum of the  $5d$  function. The spin-polarized radial functions in Fig. 3 follow the exchange-polarization rules observed by Freeman and Watson.<sup>18</sup> Here the  $5d$  spin-up function experiences a net exchange attraction to the spin-up  $4f$  electrons which pulls them radially inward. The  $5d$  spin-down functions have a zero exchange interaction with the  $4f$  electrons in Gd and are not so affected. What is clear from Fig. 3 is that the net  $5d$  radial spin density (spin-up density minus spin-down density) is negative in the outer regions

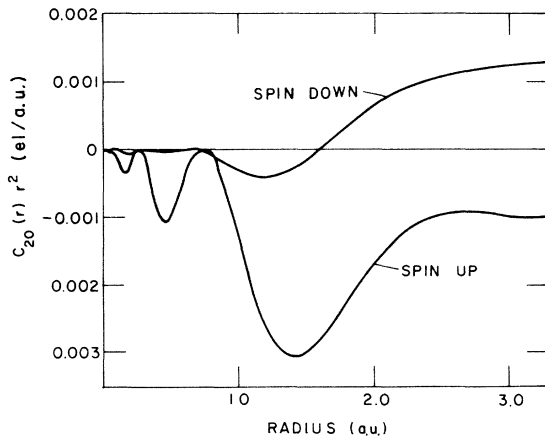


FIG. 5. The  $l=2$  nonspherical charge distributions for Gd metal.

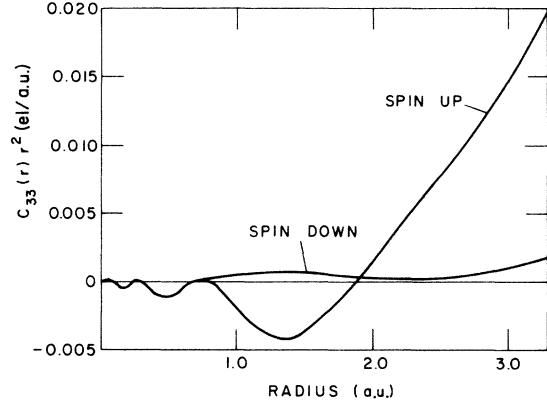


FIG. 6. The  $l=3$  nonspherical charge distributions for Gd metal.

(large  $r$  values) in a free atom for which the up- and down-spin orbitals are equally occupied.

The spin density for the crystal was obtained from the spin-up and spin-down charge densities which were calculated from a sum of occupied wave functions. The spherically averaged densities are shown in Fig. 4. The increase in the charge density near the sphere radius is from the  $l=0$  and  $l=1$  character of the wave functions, while the large shoulder (at the maximum of the atomic  $5d$  function) comes from the  $l=2$  character of the states. Subtraction of the two densities nearly removes the  $l=0$  character and gives a spin density of predominantly  $d$  character.

The nonspherical contributions to the charge density are shown in Figs. 5–7. Here the charge density has been expanded inside the APW sphere as

$$\rho(\vec{r}) = \sum_{l,m} C_{lm}(r) Z_{lm}(\hat{r}). \quad (10)$$

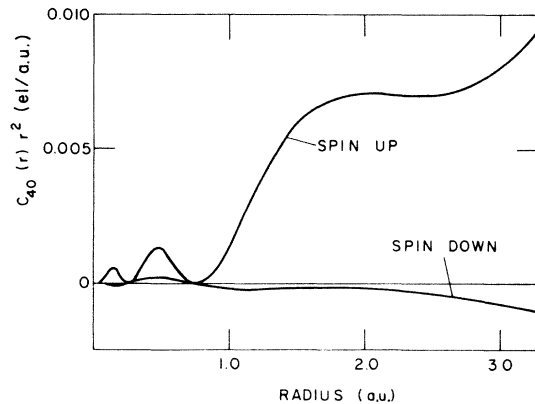


FIG. 7. The  $l=4$  nonspherical charge distributions for Gd metal.

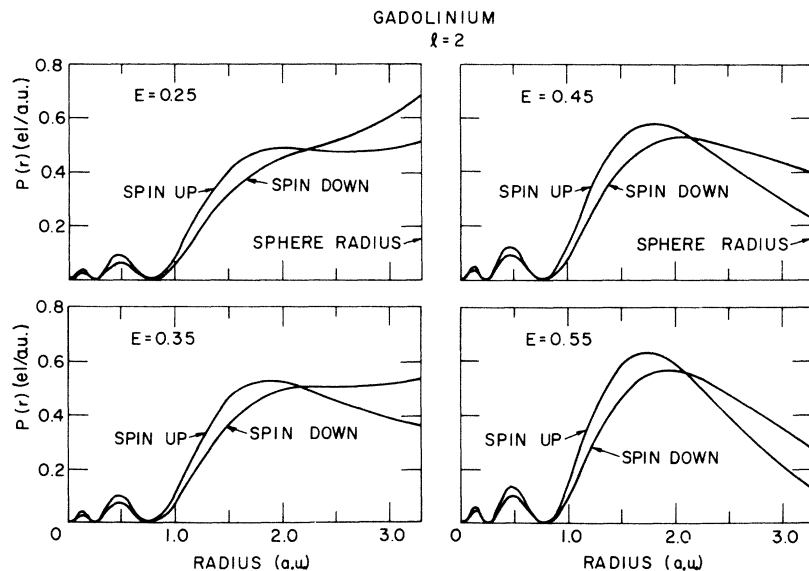


FIG. 8. The  $l=2$  spin-up and spin-down radial densities as a function of energy.

The  $Z_{lm}(\hat{r})$  are lattice harmonics and are defined in the Appendix, where we also discuss the sensitivity of the density to small improvements in the potential. For calculating the wave functions, we have used the warped-muffin-tin approximation since the aspherical densities were found to be sensitive to the nonflat potential in the interstitial region. The  $C_{53}$ ,  $C_{60}$ , and  $C_{66}$  densities did not give contributions as large inside the spheres and are therefore not shown. These figures indicate that the largest nonspherical contribution to both the total charge density and the spin density has  $l=3$  character. The  $l=3$  contributions to the density result from the mixed  $l=1$  and  $l=2$  character of the wave functions (not from  $l=2$  and  $l=3$  character as might be expected for a system with  $f$  electrons. All the wave functions were found to have less than 3%  $l=3$  character.) The large  $l=3$  term and the significant  $l=4$  term cause the spin density around each atomic site to point toward the nearest-neighbor site.

Although the spin density of Fig. 4 was found to be of predominantly  $d$  character it does not closely resemble the atomic  $d$  radial function of Fig. 3. This is easily explained by Fig. 8 where we plot the  $l=2$  radial density for several different energies. At the Fermi level the occupied  $d$  bands are very extended, and only when the energy is raised well into the unoccupied states does the  $l=2$  radial function begin to resemble the atomic  $5d$  radial function.

The greater splitting of the  $d$  bands as compared to the  $s$ -like bands can be understood from Fig. 9 where we plot the radial function for a typical  $d$  state at the Fermi energy, and for the  $\Gamma_1$   $s$ -like

state. The overlap of the  $d$  state with the  $4f$  orbital is obviously greater than that for the  $s$ -like state, and as the energy is increased (Fig. 8) the  $d$ - $4f$  overlap will increase and cause greater exchange energy splittings. The greater  $4f$ - $d$  exchange interaction is also obtained from atomic calculations and confirmed by atomic-spectroscopy measurements. The strong  $4f$ - $d$  interaction and the large amount of  $d$  character at the Fermi level suggest that the indirect exchange interaction which couples the  $4f$  local moments is dominated by  $d$  electrons—a conclusion borne out by the following

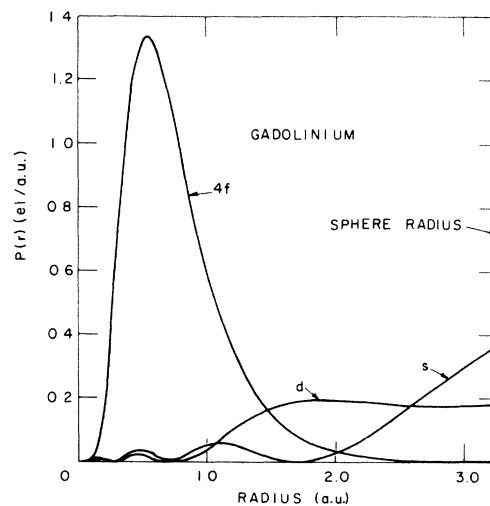


FIG. 9. Typical radial densities of  $s$ -like ( $\Gamma_1$  state) and  $d$ -like wave functions, showing overlap with the  $4f$  states.

calculation.

The strength of the  $4f$ -conduction-electron exchange interaction can be calculated exactly by evaluating the following exchange integral<sup>2</sup>:

$$J_{n,n'}(\vec{k}, \vec{k}') = \sum_{m=-3}^{+3} \int \psi_{n\vec{k}}^*(\vec{r}_1) \varphi_{4f,m}^*(\vec{r}_2) \times \frac{2}{r_{12}} \varphi_{4f,m}(\vec{r}_1) \psi_{n'\vec{k}'}(\vec{r}_2) d^3r_1 d^3r_2, \quad (11)$$

where  $n, n'$  denote the band indices. This integral is familiar from Ruderman-Kittel-Kasuya-Yosida (RKKY) theory, but has never before been evaluated using *ab initio* Bloch wave functions. By taking advantage of the fact that the  $4f$  radial functions are essentially zero in the interstitial region, the integral is easily evaluated inside the muffin-tin spheres using APW wave functions. Note that the Slater exchange approximation cannot be used to estimate this integral since separating the  $4f$  density out of the total density is incorrect for a nonlinear operator like  $\rho^{1/3}$ . We find that  $J_{n,n}(\vec{k}, \vec{k}) \approx 0.5$  eV for a pure  $d$  state on the paramagnetic Fermi surface, and  $J_{n,n}(\vec{k}, \vec{k}) \approx 0.2$  eV for the  $\Gamma_1$   $s$ -like state. This confirms our previous qualitative arguments concerning the relative strengths of the  $4f$ - $s$  and  $4f$ - $d$  interactions. Detailed calculations of  $J_{n,n'}(\vec{k}, \vec{k}')$  and the generalized susceptibility are in progress; results will be reported in a future publication.

### III. NEUTRON MAGNETIC FORM FACTOR

#### A. Experiment

The experimental form factor as obtained by Moon *et al.*<sup>4</sup> is shown in Fig. 10 together with the

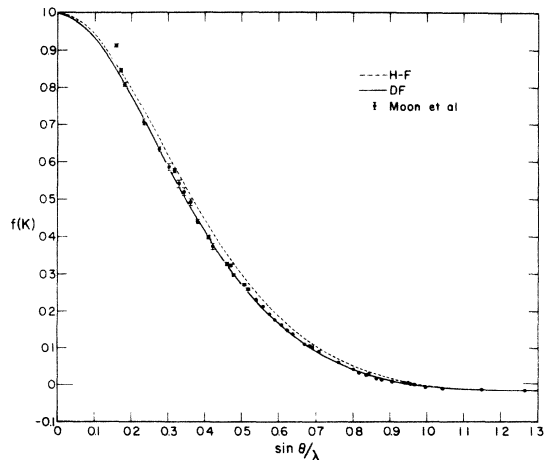


FIG. 10. Comparison of atomic form factors derived from Hartree-Fock (Ref. 18) and Dirac-Fock (Ref. 19) calculations with the Moon *et al.* (Ref. 4) experimental data.

form factors derived from the Hartree-Fock<sup>18</sup> and the Dirac-Fock<sup>19</sup> densities calculated for gadolinium. The theoretical curves represent the contribution expected of the  $4f$  electrons assuming the  $4f$  radial functions are unchanged by the solid environment. This figure shows that for large scattering angles (where the contribution from the diffuse conduction electrons is expected to be negligible) the relativistic atomic calculation is in excellent agreement with experiment. The relativistic corrections cause the inner core orbitals to contract and thus shield the nuclear charge more effectively. This in turn causes the  $4f$  radial function to expand and is reflected in the contraction of the form factor.

Moon *et al.*<sup>4</sup> devised a consistent and clever method to subtract the  $4f$  contribution from the total form factor and thus obtain the conduction-electron form factor. They assumed, however, that the  $4f$  radial function was spherically symmetric in the solid. Although a spherical  $4f$  distribution seems very reasonable, and is undoubtedly nearly correct, any nonspherical contribution which changed the  $4f$  form factor by 1% would be attributed to the conduction electron form factor as a 13% effect. This is because the ratio of the total  $4f$  moment ( $7\mu_B$ /atom) to the conduction electron total moment ( $0.55\mu_B$ /atom) is 13:1. Figure 11 shows the separation of the measured form factor into a local form factor (the straight line) and a diffuse form factor (shown in the inset), which is nonzero for only the first three reflections. The first reflection [ $\vec{k} = (1, 0, 0)$ ] is responsible for the magnitude of the derived spin density in the basal plane. It may be helpful to think of the net magnetic moment [ $\vec{k} = (0, 0, 0)$ ] of the conduction electron as determining an average value, and of the first reflection as producing a cosine modulation, with the amplitude given by the value of the first reflection. If one assumes along with Moon *et al.* that a reasonable empirical  $4f$  local

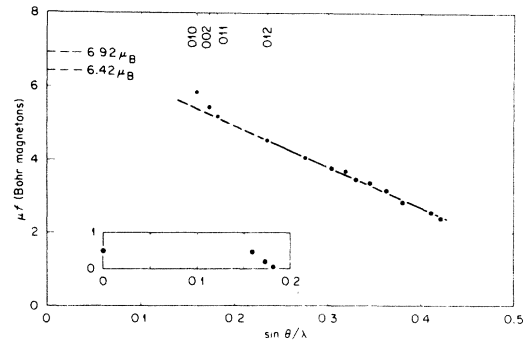


FIG. 11. Separation of the measured form factor into local and diffuse parts (from Ref. 4).

form factor has been obtained and subtracted, then the challenge is to understand the diffuse form factor and the conduction-electron polarizations responsible for it.

Inverting their derived form factor for the conduction electrons, Moon, Koehler, Cable, and Child obtained the spin-density projections shown in Fig. 12. There are large regions of negative density in the unit cell farthest from the atomic sites. The negative density reaches a maximum of  $-0.037\mu_B/\text{\AA}^3$  at the *c* site (in fcc stacking the layers are ordered *ABCABC...*, but in the hcp structure the ordering is *ABABAB...*, with the *c* sites unoccupied). Moon *et al.* comment that the derived spin density is not as expected for either an atomic *5d* or *6s* electron.

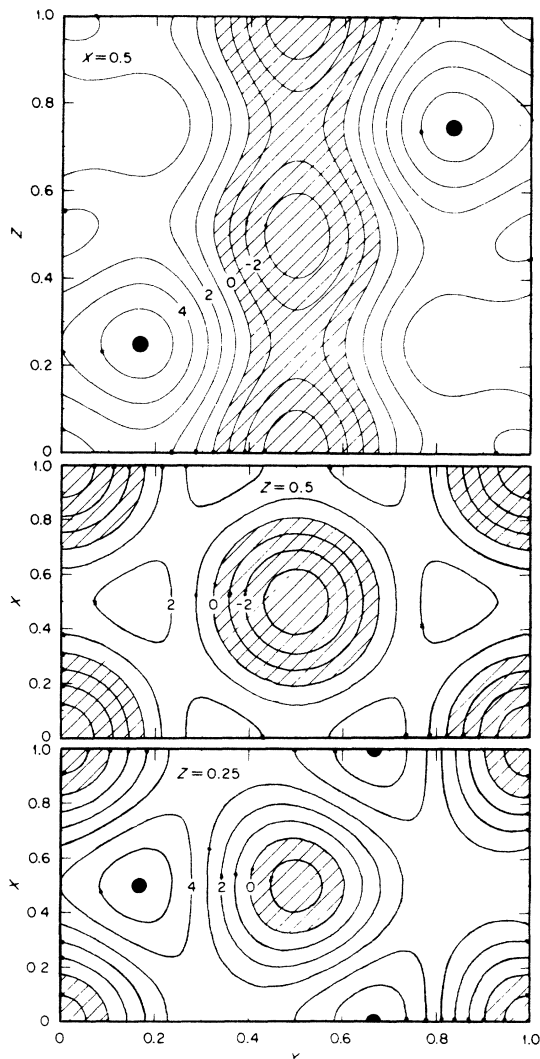


FIG. 12. Derived experimental spin-density projections (from Ref. 4). The units are  $0.01\mu_B/\text{\AA}^3$ .

### B. Theory

Contours of the calculated spin density in the basal plane are shown in Fig. 13. The expansion of the spin density (in plane waves) outside the APW spheres has been extended inside the spheres (the shaded regions), where the continuity of the wave functions and their near continuity in slope make this expansion a good representation for the basal plane. It is not, however, a good representation close to the atomic sites. The shape of the spin density shown in Fig. 13 is essentially the same as the experimentally derived density of Fig. 12 ( $Z=0.5$ ), but the magnitude is considerably smaller. For example, the calculated density at the *c* site is  $-0.002\mu_B/\text{\AA}^3$ . The spin-up density at this site is  $0.043\mu_B/\text{\AA}^3$  and the spin-down density is  $0.045\mu_B/\text{\AA}^3$  implying that a major shift of charge is required to obtain the experimental value ( $-0.037\mu_B/\text{\AA}^3$ ). The general agreement in shape is, however, a good indication that it is the spread out *d*-like conduction electrons which are contributing most to the neutron magnetic-form-factor results.

The wave-function character at the paramagnetic Fermi surface is the most significant factor in determining the character of the spin density because as the bands are split the spin-up states at the Fermi surface are no longer compensated by similar spin-down states. The uncompensated states in gadolinium all have over 90% *d* character with some *p* and a little *s* character as well. This helps explain the predominant *d* character of the spin density, but by itself could not explain the negative density region.

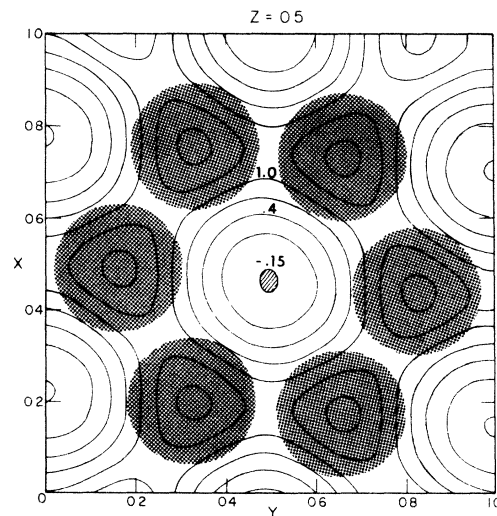


FIG. 13. Calculated spin density in the basal plane in units of  $0.01\mu_B/\text{\AA}^3$ . The shaded regions are inside the APW spheres.

The negative density is a result of the radial exchange splitting for the compensated spin-up and spin-down wave functions. This is essentially the atomic picture shown in Fig. 3. However, the spin density one might expect from these atomic  $5d$  orbitals does not resemble the spherically averaged spin densities of the metal (Fig. 4), since the occupied  $d$  states are at the very bottom of the  $d$  bands. The  $l=2$  radial dependence for various energies was shown in Fig. 8. At the lowest energy  $E=0.25$  Ry the spin-up bands are just beginning to be occupied. At  $E=0.35$  Ry we are near the Fermi energy, so this is the  $l=2$  dependence of the uncompensated states and closely resembles the spherically averaged spin density of Fig. 4.

The contribution from inside the APW spheres to the calculated magnetic form factor was obtained using the expansion of the spin density given in Eq. (10) for  $l$  up to 6. The contribution from outside the spheres was easily obtained since the spin density is expanded in plane waves in this region. The calculated form factor is given in Table I for the calculation using full Slater exchange ( $\alpha=1$ ) as well as for the calculation using the Kohn-Sham-Gaspar value of exchange ( $\alpha=\frac{2}{3}$ ). Both calculated form factors are much smaller at non-zero-scattering angles than the form factor derived by Moon *et al.* This could be expected by comparing the spin densities, since the smaller changes in magnitude of the calculated spin density imply smaller scattering for  $(\sin\theta)/\lambda \neq 0$ . The form factor from the  $\alpha=\frac{2}{3}$  calculation has very little scattering for  $(\sin\theta)/\lambda \neq 0$  because the lowered exchange does not split the (more expanded)  $5d$  radial functions as much as

for  $\alpha=1$  calculation and hence the spin density is more uniformly spread through the unit cell. Thus the form factor is contracted, and, except for the first reflection, we are now looking at the tail of the form factor as it falls below zero. In spite of this expansion of the  $\alpha=\frac{2}{3}$  spin density, the shape remains pretty much identical to the  $\alpha=1$  density, and the  $d$  character is still dominant. The negative regions have disappeared, with the magnitude of the spin density at the  $c$  site being  $+0.003\mu_B/\text{\AA}^3$ . Possible reasons for this lack of agreement in magnitude are discussed in Sec. IV.

#### IV. ADDITIONAL CONTRIBUTIONS TO THE MAGNETIZATION DENSITY AND NEUTRON MAGNETIC FORM FACTOR

Our *ab initio* determination of the conduction-electron spin density in ferromagnetic Gd metal yielded a form factor which differed from the experimental value. The magnitude of the "diffuse" spin density derived by Moon *et al.*<sup>4</sup> was found to be larger than the magnitude calculated from the APW wave functions, although the shapes of the two spin densities agreed very well. Since neutrons scatter from the *total* magnetic-moment density, effects such as core polarization and spin-orbit mixing could give rise to important contributions to the form factor. In this section we discuss aspects of the magnetic-moment density which were not considered previously.

##### A. Core polarization

The net magnetic moment in gadolinium is determined by the number of uncompensated valence

TABLE I. Comparison of the gadolinium conduction-electron form factors for the first ten reflections.

Reflection ( $hkl$ )	$\sin\theta$ $\lambda$	expt. <sup>a</sup>	expt. <sup>b</sup>	$\alpha=\frac{2}{3}$	$\alpha=1$	$\alpha=1$ with core pol.	Aspherical contributions	
							$\alpha=1$ $Z_{33}$	$\alpha=1$ $Z_{40}$
(000)	0.000	1.000	1.000	1.000	1.000	1.000	0.000	0.000
(010)	0.159	0.930	0.770	0.184	0.385	0.531	0.040	0.004
(002)	0.173	0.428	0.218	0.048	0.263	0.431	0.000	0.014
(011)	0.181	0.096	-0.064	-0.009	0.140	0.293	-0.011	-0.004
(012)	0.235		-0.103	-0.063	0.049	0.194	0.018	-0.010
(110)	0.276		-0.051	-0.057	0.022	0.145	0.000	0.014
(013)	0.304		-0.014	-0.050	0.004	0.098	-0.002	-0.002
(020)	0.319		0.244	-0.056	0.005	0.092	0.025	0.016
(112)	0.325		...	-0.071	-0.027	0.053	0.000	-0.007
(021)	0.330		0.64	-0.072	-0.022	0.043	0.005	0.005
(004)	0.345		0.14	-0.029	0.016	0.070	0.000	0.044

<sup>a</sup> Estimated from Fig. 5 of Moon *et al.* (Ref. 4).

<sup>b</sup> Obtained by subtracting the Freeman-Desclaux (Ref. 19) local form factor from the measured form factor.

electrons and their orbital angular momentum (if any). The spin density, however, has contributions from the core electrons as well. The large exchange interaction with the local  $4f$  states pulls spin-up orbitals towards the peak in the  $4f$  density, as shown in Fig. 8; the radial densities of spin-up and spin-down core electrons are thus split, and contribute to the spin density.<sup>20, 21</sup>

The  $5s$  and  $5p$  radial functions are peaked outside the high-density region of the  $4f$  electrons and extend to some degree into the interstitial region. The other core states in gadolinium are more localized than the  $4f$  states, so their spin distribution only affects high-angle reflections in the form factor. Since  $5s$  and  $5p$  states from neighboring lattice sites overlap, they actually form bands in the solid with a band width of about 1 eV. Thus their spin density may be calculated using the APW method.

The  $5s$  and  $5p$  wave functions were calculated using the  $\alpha=1$  potential. The spin density was found to be negative in the interstitial region, but very small ( $-0.001\mu_B/\text{\AA}^3$  at the  $c$  site). Figure 14 shows the spin-polarized  $5p$  densities for the metal and illustrates the amount of exchange splitting. The calculated atomic  $5s$  and  $5p$  magnetic form factors are shown in Fig. 15. In this figure the  $5p$  form factor should be multiplied by three to obtain the total for all six  $5p$  electrons. The form factors for the solid were slightly reduced. They are not shown because they exist only at the Bragg scattering angles and a better understanding of them can be obtained with the continuous atomic form factor.

The  $5s$  and  $5p$  core-polarization corrections have been added to the conduction-electron form factor from the  $\alpha=1$  potential and the result is

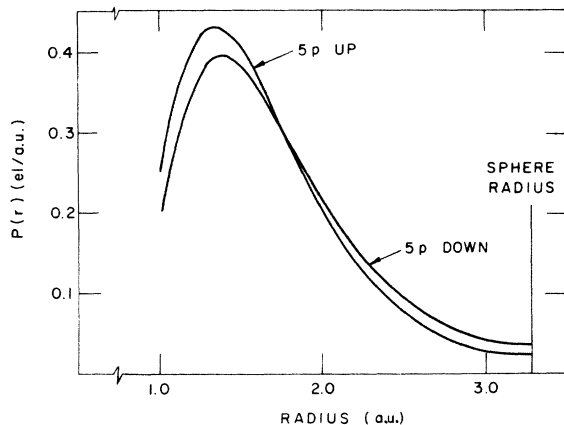


FIG. 14. Spin-up and spin-down radial density for the  $5p$  states determined from the spin-polarized APW calculation for Gd metal.

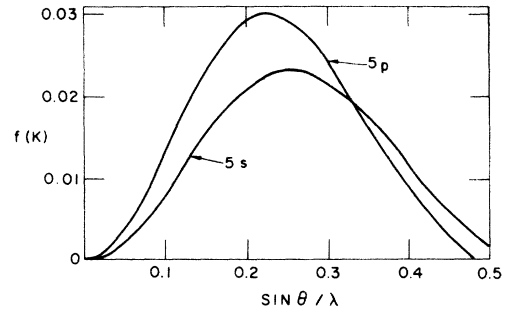


FIG. 15. Contributions to the magnetic form factors from the  $5s$  and  $5p$  states in ferromagnetic Gd metal.

shown in Table I. Since the  $5s$  and  $5p$  form factors are rather broad, their main effect is to uniformly raise the conduction-electron form factor for the smaller reflections. Although these changes are hardly noticeable on the scale of the total magnetic form factor, the corrections are significant on the scale of the "diffuse" form factor. Table I shows that the  $\alpha=1$  form factor with core polarization included is in better agreement with Moon *et al.*,<sup>4</sup> but that the calculated first reflection is still too low.

#### B. Relativistic effects

The need for including relativistic effects in the calculation of  $4f$  spin density and form factor has been discussed earlier. In the relativistic calculation the inner core states contract and the resultant increase in screening allows the  $4f$  density to expand. An estimate of the changes in the conduction-electron densities caused by these indirect relativistic effects can be made by comparing the atomic relativistic Dirac-Slater radial densities with the nonrelativistic Hartree-Fock-Slater results. This comparison is made in Table II. The relativistic corrections cause the  $5d$  density to expand in a manner similar to the  $4f$  re-

TABLE II. Radial expectation values (a.u.) for relativistic and nonrelativistic atomic calculations of Gd.

Orbital	$\langle r^2 \rangle^{1/2}$	$\langle r^4 \rangle^{1/4}$	$\langle r^6 \rangle^{1/6}$
Hartree-Fock-Slater			
6s	4.52	5.12	5.74
5d	2.62	3.15	3.74
4f	0.87	1.09	1.34
Dirac-Slater			
$6s^{1/2}$	4.25	4.83	5.43
$5d^{5/2}$	2.77	3.38	4.06
$4f^{7/2}$	0.92	1.17	1.46
$4f^{5/2}$	0.91	1.15	1.43

sult, and the 6s density to contract. Similar behavior is expected in the solid, since the core region, where direct relativistic effects are important, is little changed in the metal. A very small expansion of both 5d-up and 5d-down wave functions would cause the form factor to contract, but the change would be small and of little significance. (Recall that we are dealing with the difference of two charge densities, both of which are affected similarly by these indirect relativistic effects.)

Spin-orbit coupling is another relativistic correction which can affect the magnetic-moment density. The crystal field normally quenches the angular momentum of the conduction electrons, but spin-orbit coupling causes the spin to "drag along" some orbital moment. The amount of orbital mixing is found experimentally by measuring the  $g$  factor of the conduction electrons. The percent of orbital mixing is then given by  $\frac{1}{2}(g-2)$ . It is difficult to decide on a  $g$  value for the conduction electron since most measurements are dominated by the 4f shell and its magnetic interactions. Some orbital contribution to the magnetic-moment density can be expected, but we have been unable to determine how much.

The general shape of the orbital form factor for the metal can be inferred from atomic Hartree-Fock calculations. Both the spin and orbital form factors for the atomic 5d state are shown in Fig. 16. The difference is also plotted, and indicates that if the percent of orbital contributions were significant, the smaller reflections could be raised above the spin-only values. These atomic 5d form factors should be approached with some caution, however, since the shape of the occupied  $d$  states in Gd (Fig. 8) does not resemble the shape of 5d atomic states (Fig. 3). If one assumes that the conduction-electron  $g$  factor in Gd is the same as the  $g$  factor of the ferromagnetic transition metals ( $g \approx 2.2$ ), then there would be a 10% orbital contribution. This would raise the first 10 reflections given in Table I by about 0.02. This is a rather small amount and indicates that orbital mixing would have to be quite large to make a significant contribution (at least at the precision of the present measurements). As noted previously, the direction of an orbital moment could be opposite to the spin-moment direction as happens in  $L$ - $S$  coupling for less than half-filled shells. This is an interesting possibility and could lead to significant contributions. The size of the conduction-electron orbital moment is thus quite important if the orbital contributions to the form factor are to be determined.

Perhaps the best way to obtain the orbital contribution would be to use relativistic APW wave

functions for which spin-orbit coupling is treated in a natural way. The problem with this approach is the creation of a suitable ferromagnetic potential in the relativistic formalism where spin is no longer a good quantum number, and  $L$ - $S$  coupling for the 4f states is no longer valid.

We conclude that while indirect relativistic effects are not important for the conduction electrons, spin-orbit effects could be important, but only if the orbital mixing is rather large.

### C. Interband mixing

Interband mixing has been suggested as a mechanism to explain the apparent negative electron polarization for a number of rare-earth metallic compounds.<sup>22, 23</sup> The APW method should in principle be able to describe interband hybridization effects properly; however, there are a number of practical aspects which cause difficulty. First and foremost is the description of the highly localized 4f states as bands. The neglect of the Coulomb correlation makes the location in energy of the 4f states unreliable in an APW calculation. The location in energy of these states is further complicated by their extreme sensitivity to changes in the Slater exchange scaling parameter  $\alpha$ . For example, the spin-up 4f energy was  $-0.8$  Ry using  $\alpha=1$ , but was raised to  $-0.15$  Ry (0.25 Ry below the conduction bands) using  $\alpha=\frac{2}{3}$ . With the  $\alpha=\frac{2}{3}$  potential the 4f spin-down bands are lowered to an energy just above the Fermi level.

The amount of  $l=3$  character in the spin-up

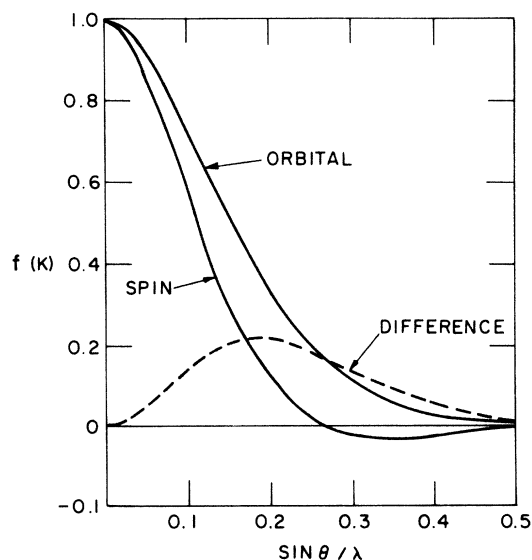


FIG. 16. Spin and orbital form factors for the atomic 5d wave function of gadolinium together with their difference.

wave functions was found to never be more than 3% for both the  $\alpha=1$  and  $\alpha=\frac{2}{3}$  calculations. There was some  $l=3$  character in the occupied  $\alpha=\frac{2}{3}$  spin-down wave functions due to the proximity of the  $4f$  spin-down bands to the Fermi energy. Since photoemission experiments place the occupied  $4f$  levels in Gd at 6eV below the Fermi energy (approximately the energy level given in the  $\alpha=\frac{2}{3}$  calculation), we conclude that in Gd metal there is no significant interband mixing with the  $4f$  spin-up states. The effect of the  $4f$  spin-down interband mixing observed for the  $\alpha=\frac{2}{3}$  calculation was to pull spin-down density out of the interstitial region and into the core region. This is understandable since some of the occupied spin-down states now have significant  $l=3$  character. The  $l=3$  spin-down radial function near the Fermi level is only slightly expanded relative to the  $4f$  spin-down states; hence, the states with mixed  $l=3$  character give up some diffuse character in return for localized  $l=3$  character. Since the experiment of Moon *et al.*<sup>4</sup> indicated large amounts of negative density in the interstitial region we can assume that there is little interband mixing with  $4f$  spin-down states. We conclude therefore, that interband mixing with the  $4f$  states is insignificant in gadolinium metal.

#### D. Nonspherical contributions

The spin, orbital, and core-polarization form factors shown in Figs. 15 and 16 are derived from spherically symmetric densities and vary smoothly from  $(\sin\theta)/\lambda=0$  to high reflections. However, the first three reflections of the experimental data in Fig. 11 indicate a very large change in the form factor over the relatively small difference in scattering angles of the first three reflections. Such a precipitous drop cannot be understood as arising from spherical densities as obtained from atomic form factors.

The nonspherical terms of the spin density have been included in our calculations, but as discussed in the Appendix, these contributions to the density are most sensitive to potential approximations. The contributions inside the muffin-tin sphere to the form factor for terms proportional to  $Z_{33}(r)$  and  $Z_{40}(r)$  are included in Table I. These are for the  $\alpha=1$  warped-muffin-tin potential. It can be seen from the table that the  $Z_{33}(r)$  terms act to shift the first three reflections in the direction obtained experimentally, but these changes are not large enough by themselves to give the observed shift. An idea of how large the nonspherical spin density must be to obtain the form factor of Fig. 10, may be obtained by calculating the following quantity:

$$C_{lm}(R) = \int S(\hat{R}) Z_{lm}(\hat{R}) d^2r,$$

where  $S(\hat{R})$  is the spin density at the muffin-tin radius derived from the form factor of Fig. 10. These  $C_{lm}$ 's are compared in Table III, with the  $C_{lm}$ 's calculated using the APW spin densities. The experimental  $C_{33}(R)$  and  $C_{40}(R)$  are exceptionally large, as might be expected from the steep slope in the form factor for the first three reflections. That they are 3 to 4 times the calculated values is surprising.

The potentials used to calculate the charge and spin densities were formed by overlapping the atomic charge densities from neighboring sites. These potentials do not have the large aspherical spin dependence that is calculated from the wave functions. Hence a general self-consistent potential which avoided all muffin-tin approximations would be expected to further increase the nonspherical densities. Since most of the  $d$ -like wave functions have about 60% of their charge inside the APW spheres, it is especially important to include nonspherical contributions inside the APW sphere (not just in the interstitial region as is done with the warped-muffin-tin approximation). Judging from the changes in the nonspherical contributions to the charge density caused by the ad-

TABLE III. Effects of warped-muffin-tin potential on  $C_{lm}(R)$  [Eq. (A1)]. The  $C_{lm}(R)$ 's have been multiplied by the volume of the unit cell. Note the large nonspherical terms for the spin density of Moon *et al.* (Ref. 4). The units are 440e1/a.u. (Ref. 3).

		Charge density					
		MT		WMT		WMT	
		$\alpha=1$		$\alpha=1$		$\alpha=\frac{2}{3}$	
$l$	$m$	up	down	up	down	up	down
0	0	10.300	7.990	10.291	8.094	11.484	8.264
2	0	-0.021	-0.066	-0.038	0.055	0.180	-0.002
3	3	0.411	-0.493	0.822	0.073	0.717	0.046
4	0	0.170	-0.284	0.397	-0.036	0.175	-0.133
5	3	-0.137	-0.312	0.031	-0.122	-0.147	-0.345
6	0	0.061	0.090	0.027	0.065	0.154	0.142
6	6	0.058	0.071	0.016	0.031	0.066	0.053

		Spin density			
		MT	WMT	WMT	Moon
		$\alpha=1$	$\alpha=1$	$\alpha=\frac{2}{3}$	<i>et al.</i> <sup>4</sup>
$l$	$m$				
0	0	2.316	2.197	3.220	2.055
2	0	0.045	-0.093	0.182	0.000
3	3	0.904	-0.749	0.671	2.918
4	0	0.454	0.433	0.308	1.193
5	3	0.175	0.153	0.198	0.554
6	0	-0.029	-0.038	0.012	0.148
6	6	-0.013	-0.015	0.013	-0.159

dition of only the warped-muffin tin corrections in the interstitial potential, we believe that a full general self-consistent potential would be the most important consideration for improving our results.

The large anisotropy of the conduction-electron spin density could also cause the core and  $4f$  spin densities to assume a small amount of asphericity. Thus, separating out a form factor due to a local spherical moment as was done by Moon *et al.* may not be a valid procedure. As stated earlier, a 1% aspherical contribution from the local moment would be interpreted as a 13% aspherical contribution from the conduction electrons. The determination of aspherical local-moment contributions must await the development of a general (non-muffin-tin) self-consistent potential.

Finally, we should emphasize that the "true" conduction-electron polarization and spin density is produced not by a simplified  $\rho^{1/3}$  spin polarization but by the much more complex (and nonlocal)  $J(\vec{k}, \vec{k}')$  exchange interaction [e.g. Eq. (11)]. Our preliminary calculations using our APW band eigenfunctions of the  $4f$  and  $5d$  electrons in the paramagnetic state show that  $J(\vec{k}, \vec{k}')$  is strongly dependent on  $\vec{k}$  and  $\vec{k}'$  and on the band indices  $n, n'$ . This highly anisotropic exchange interaction could well produce ferromagnetic magnetization densities showing the right amount of asphericity and a higher first reflection could well result. Such a band-type calculation using the correct  $J(\vec{k}, \vec{k}')$  is, however, not easily accomplished at the present time.

## V. CONCLUSIONS

Highly precise experiments, such as the neutron-magnetic-scattering experiments of Moon *et al.*, on the rare-earth metals, which measure physical phenomena requiring wave functions as opposed to eigenvalues for their description, are relatively new; furthermore, the interaction between theory and experiment has only just started. Eigenvalues and energy bands are not as sensitive as wave functions to potential approximations and are therefore less likely to provide as much detailed knowledge of electronic interactions in solids. Thus the study of phenomena requiring wave functions for their description may well be the key to assessing the limits of the single particle model and to understanding the role of many-body effects.

This paper was concerned with understanding what considerations are important for an accurate single-particle description of the spin density of gadolinium. The comparison of the APW calculations with the experimental results has provided

insight into the conduction-electron interactions. Before such comparisons can be made, however, the quality and properties of the wave functions must be known. This is the reason for the importance of the investigations presented in the Appendix and in a previous publication.<sup>24</sup> The rapid convergence found for matrix elements calculated using APW wave functions (for a fixed potential) is important for saving computer time and space. The sensitivity to potential found for the nonspherical part of the wave functions is also important for comparing theory with experiment. In addition, the sensitivity of the nonspherical part of the wave function may explain why self-consistent muffin-tin calculations can give good eigenvalues (eigenvalues depend primarily on the spherical density) but can give poor charge densities.

The most significant discovery to come from these calculations is the prominence of the  $d$  electrons in determining the magnetic properties of the rare-earth metals. The nearly complete  $d$ -like character of the wave functions found at the Fermi level accounts for the  $l=2$  character of the conduction-electron spin density, and helps explain the poor electrical conductivity of the rare-earth metals. The  $d$  character at the Fermi surface and the dominant  $4f$ - $d$  exchange interaction found by the calculations imply that the coupling of the  $4f$  local moments below the ordering temperature, is solely determined by  $d$  electrons.

It was found that the splitting of the compensated spin-up and spin-down radial densities is responsible for the negative spin density at the  $c$  site in the unit cell. The radial densities of  $s$ -like electrons are split very little because of the smaller  $4f$ - $s$  exchange interaction. The exchange interaction of the  $s$  electrons with the other conduction electrons can be large, but the exchange interaction from the diffuse density of the conduction electrons does not "push" or "pull" in any particular direction. Thus there is very little  $s$ -like character to spin density.

Although the calculated spin density has the same shape as the "diffuse" density of Moon *et al.*,<sup>3</sup> the magnitudes of the two do not agree. Part of this difference was shown to be from core-polarization contributions, and much of the remaining difference can be attributed to nonspherical contributions. Since the angular part of APW wavefunctions was found to be sensitive to anisotropies in the potential, a calculation using a better potential would increase the calculated nonspherical terms. Also, the nonspherical terms of the "diffuse" density of Moon *et al.*, could be reduced, if, as seems likely, there is a small nonspherical contribution which could be attributed to the local

density. These large nonspherical densities found for a hexagonal-close-packed metal imply that for calculating charge and spin densities the muffin-tin potential must be approached with caution. This will be particularly true for calculations describing experiments which stress wave-function properties, such as positron annihilation distributions, Compton profiles, and crystal-field effects.

#### ACKNOWLEDGMENTS

The authors would very much like to thank D. D. Koelling for many helpful discussions pertaining to the computational aspects of the problem, and the staff of the Vogelback Computing Center for their excellent service.

#### APPENDIX

The convergence properties of APW eigenvalues are fairly well known, but the wave-function properties have not received as extensive a study. We have commented on the convergence properties of APW wave-functions for a given fixed potential in a previous publication<sup>24</sup> and will be concerned here only with the sensitivity of the wave functions to small changes in the potential. In particular we wish to point out how the wave functions change when warped-muffin-tin corrections are included in the APW secular equation.

The standard muffin-tin approximation assumes a spherically averaged potential inside the spheres and a zero potential in the interstitial region. The warped-muffin-tin approximation still assumes a spherically averaged potential inside the spheres, but uses the actual potential in the interstitial region. Since the APW basis set in the interstitial

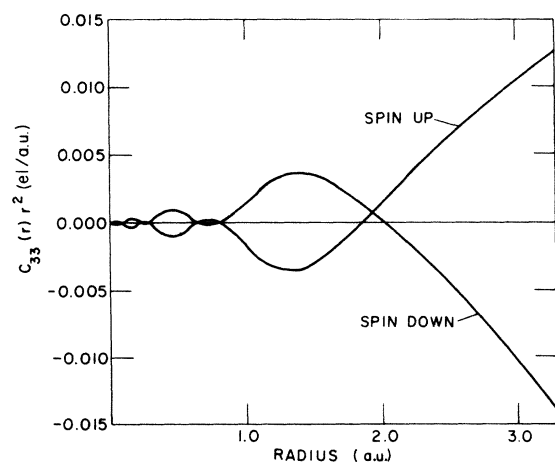


FIG. 17. The  $l=3$  nonspherical charge distributions obtained in the APW calculation using the muffin-tin potential.

region consists of just plane waves, the matrix elements are easily expressed as

$$M_{ij} = \int e^{-i\vec{k}_i \cdot \vec{r}} V_{\text{WMT}}(\vec{r}) e^{i\vec{k}_j \cdot \vec{r}} d^3r,$$

or

$$M_{ij} = V(\vec{k}_{ij}),$$

where

$$V_{\text{WMT}}(\vec{r}) = 0, \quad |\vec{r}| < R_{\text{MT}}$$

and  $\vec{k}_{ij} = \vec{k}_j - \vec{k}_i$  is a reciprocal-lattice vector.

The construction of  $V_{\text{WMT}}(\vec{r})$  and its use in the APW method are described in Ref. 13. For fcc and bcc metals the changes in eigenvalues induced by including the warped-muffin-tin corrections are on the order of 0.005–0.01 Ry. For gadolinium the energy changes were also in this range and were not large enough to significantly change the occupation of the bands for the mesh used.

To determine to some extent the changes in the wave functions we have looked at changes in the total charge densities for both sets of bands. The charge density can be expanded as in Eq. (10) only at the sphere radius:

$$\rho(\hat{R}) = \sum_{l,m} C_{l,m}(R) Z_{lm}(\hat{R}), \quad (\text{A3})$$

where  $R$  is the sphere radius and the  $Z_{l,m}(\hat{R})$  are related to the usual spherical harmonics by

$$\begin{aligned} Z_{00} &= Y_{00}, & Z_{20} &= Y_{20}, \\ Z_{33} &= (1/\sqrt{2})(Y_{33} - Y_{3-3}), & Z_{40} &= Y_{40}, \\ Z_{53} &= (1/\sqrt{2})(Y_{53} - Y_{5-3}), & Z_{60} &= Y_{60}, \\ Z_{66} &= (1/\sqrt{2})(Y_{66} + Y_{6-6}). \end{aligned} \quad (\text{A4})$$

We have tabulated these  $C_{l,m}(R)$ 's in Table III for both muffin-tin and warped-muffin-tin potentials. As seen in the table,  $C_{00}(R)$  is insensitive to this

TABLE IV. Effect of warped-muffin-tin potential on  $C(\vec{K}_s)$  [Eq. (A5)]; the  $C(\vec{K}_s)$  have been multiplied by the volume of the unit cell. The units are 440el/a.u. (Ref. 3).

$\vec{K}_s$	Spin up		Spin down	
	MT	WMT	MT	WMT
000	2.678	2.539	1.816	1.956
100	0.316	0.037	0.909	0.486
110	0.119	0.162	0.085	0.115
200	-0.012	-0.017	-0.039	-0.058
101	1.774	1.904	1.068	1.415
002	0.322	0.210	0.312	0.316
102	-0.314	-0.498	-0.052	-0.275
114	-0.124	-0.099	0.051	0.041
211	0.191	0.188	0.071	0.100

correction. The spherically averaged charge density calculated with the warped-muffin-tin wave functions was essentially identical to the muffin-tin density. The total charge inside the spheres was increased by less than 1%. This kind of insensitivity is not observed for the other coefficients. In particular the  $C_{33}(R)$  gives dramatic evidence that the nonspherical components of the charge density can be completely wrong, using the muffin-tin approximation. In Fig. 17 we show  $C_{33}(r)r^2$  for the muffin-tin potential. Comparison with the warped-muffin-tin results of Fig. 6 shows the dramatic shift in charge, the spin-down coefficient showing a reversal in sign. What is happening is that the warped-muffin-tin potential is rather like a landscape with hills away from the atomic sites and valleys between them. The angular dependence of the wave functions are quite sensitive to these variations which cause the highest density to settle into the valleys. The muffin-tin potential did not yield this standard text book picture of higher density between the nearest atoms.

To see these effects in the interstitial region,

we consider changes induced in the  $C(\vec{K}_s)$  expansion coefficients. These are defined in the interstitial region by

$$\rho(\vec{r}) = \sum_{\vec{K}_s} C(\vec{K}_s) S_{\vec{K}_s}^*(\vec{r}), \quad (\text{A5})$$

where  $S_{\vec{K}_s}^*(\vec{r})$  is a symmetrized plane wave. The  $C(\vec{K}_s)$  for the two potentials are given in Table IV. Again the  $C(0)$  is not greatly affected, but those coefficients with strong  $l=3$  dependence [e.g.,  $\vec{K} = (1, 0, 0)$ ] are changed considerably.

Corrections to the potential inside the spheres can be expected to enhance these changes in nonspherical densities, although based on the eigenvalue shifts we would expect these corrections to be less important. We conclude that although energy eigenvalues and spherical charge densities are adequately handled for gadolinium with the muffin-tin approximation, the nonspherical parts of the density require a potential which includes correction in the interstitial region, and may require correction inside the spheres as well.

\*Supported by the National Science Foundation, the Air Force Office of Scientific Research and the U. S. Atomic Energy Commission.

†Present address: Physics Department, Iowa State University, Ames, Iowa 50010.

<sup>1</sup>Extensive reviews of the experimental and theoretical work on the rare-earths is given in *Magnetic Properties of the Rare Earth Metals*, edited by R. J. Elliott (Plenum, London, 1972).

<sup>2</sup>For a thorough review of the electronic band structure, RKKY theory and magnetic ordering of the rare-earth metals, and detailed references to this work see A. J. Freeman (Chap. 6 of Ref. 1).

<sup>3</sup>J. O. Dimmock and A. J. Freeman, Phys. Rev. Lett. **13**, 750 (1964).

<sup>4</sup>R. M. Moon, W. C. Koehler, J. W. Cable, and H. R. Child, Phys. Rev. B **5**, 997 (1972).

<sup>5</sup>B. N. Harmon, Ph.D. thesis (Northwestern University, 1973) (unpublished).

<sup>6</sup>J. O. Dimmock, A. H. Freeman, and R. E. Watson, J. Appl. Phys. **36**, 1142 (1965). A. J. Freeman, J. O. Dimmock, and R. E. Watson, in *Quantum Theory of Atoms, Molecules and the Solid State, a tribute to John C. Slater*, edited by P. O. Lowdin (Academic, New York, 1966), 361.

<sup>7</sup>S. C. Keeton and T. L. Loucks, Phys. Rev. **146**, 429 (1966); **168**, 672 (1968); A. R. Mackintosh, Phys. Lett. **28A**, 217 (1968); C. Jackson, Phys. Rev. **178**, 949 (1969).

<sup>8</sup>J. C. Slater, Phys. Rev. **51**, 151 (1937).

<sup>9</sup>John W. D. Connolly, Int. J. Quantum. Chem. **11s**, 257 (1968).

<sup>10</sup>T. L. Loucks, *Augmented Plane Wave Method* (Benjamin, New York, 1967).

<sup>11</sup>L. F. Mattheiss, J. H. Wood, and A. C. Switendick, Methods Comput. Phys. **8**, 64 (1968).

<sup>12</sup>J. O. Dimmock, Solid State Phys. **26**, 103 (1971).

<sup>13</sup>D. D. Koelling, A. J. Freeman, and F. M. Mueller, Phys. Rev. B **1**, 1318 (1970).

<sup>14</sup>D. D. Koelling, J. Phys. Chem. Solids **33**, 1335 (1972).

<sup>15</sup>A more efficient and faster variation of this method is given by B. N. Harmon and D. D. Koelling, J. Phys. C **7**, L210 (1974).

<sup>16</sup>J. H. Wilkinson, *The Algebraic Eigenvalue Problem* (Oxford U.P., London, 1965); and J. H. Wilkinson and C. Reinsch, in *Handbook for Automatic Computation* (Springer-Verlag, New York, 1971), Vol. II.

<sup>17</sup>L. F. Mattheiss, Phys. Rev. **133**, 184 (1963).

<sup>18</sup>A. J. Freeman and R. E. Watson, Phys. Rev. **127**, 2058 (1962).

<sup>19</sup>A. J. Freeman and J. P. Desclaux, Int. J. Magn. **3**, 311 (1972).

<sup>20</sup>A. J. Freeman and R. E. Watson, in *Magnetism*, edited by G. T. Rado and H. Suhl (Academic, New York, 1964), Vol. 11A.

<sup>21</sup>A. J. Freeman and R. W. Watson, Phys. Rev. Lett. **14**, 695 (1965).

<sup>22</sup>P. W. Anderson and A. M. Clogston, Bull. Am. Phys. Soc. **2**, 124 (1961).

<sup>23</sup>R. E. Watson, A. J. Freeman, and S. Koide, Phys. Rev. **186**, 625 (1969).

<sup>24</sup>B. N. Harmon, D. D. Koelling, and A. J. Freeman, J. Phys. C **6**, 2294 (1973).

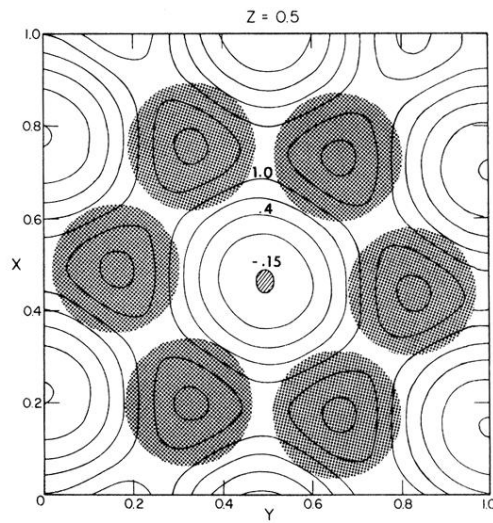


FIG. 13. Calculated spin density in the basal plane in units of  $0.01\mu_B/\text{\AA}^3$ . The shaded regions are inside the APW spheres.